



POLITECNICO MILANO 1863

ORBITAL MECHANICS

FINAL ASSIGNMENT

GROUP 9

Bardazzi, Niccolò	PC: 10800456, MN: 963039
Carcano, Stefano	PC: 10578334, MN: 887642
Domaschio, Jacopo	PC: 10530480, MN: 968568
Maestro Martínez, José David	PC: 10784894, MN: 963848

MSc in Space Engineering - AY 2020/2021

Contents

1	Interplanetary Transfer	2
1.1	Introduction	2
1.2	Preliminary Analysis	2
1.3	Grid Search	4
1.4	Optimization	7
1.5	Conclusion and solution selection	8
2	Planetary Orbit	12
2.1	Introduction	12
2.2	Ground Track	12
2.3	Moon Perturbation	14
2.4	Element evolution and Filtering	17
2.5	Comparison with real data	18
	Bibliography	22

CHAPTER 1

Interplanetary Transfer

1.1 Introduction

The aim of the first part of this report is to analyze an interplanetary transfer visiting three assigned planets and performing a powered fly-by around the intermediate one.

Hereby a discussion about the problem is presented together with a set of solutions to achieve the mission. The whole selection of transfer possibilities has been calculated using the method of *Patched-Conics*, considering a preliminary approximation: initial and arrival heliocentric orbits are equal to those of the departure and arrival planet, avoiding the planetary departure phases and the final insertion.

The final solution will meet a constraint regarding earliest departure date and latest arrival date and it will be proposed based mainly on the minimization of the total cost (in terms of Δv) of the mission.

1.2 Preliminary Analysis

The analysis starts with an overview and a presentation of the problem. In Table 1.1 are displayed the assigned planets, with their orbital periods and their semi-major axes, and the time constraints.

		Orbital Period [years]	Orbit a[km]
Departure planet	Jupiter	11.863892	778412027
Fly-By planet	Mars	1.8808	227936637
Arrival planet	Venus	0.615	108210000
Earliest departure	2029/05/01		
Latest arrival	2069/05/01		

Table 1.1: Assigned Data.

From this information, the synodic periods of the two couples of planets can be calculated separately in order to have a first approach to the problem's behaviour. It is useful to know that, if there is an advantageous departure window, there won't be another one until, at least, the repetition of the greater synodic period between two of the three planets. For example, assuming the orbits to be circular, we can approximately calculate the synodic period between

Jupiter and Mars using Equation 1.1:

$$T_{jm} = \frac{T_j T_m}{T_j - T_m} \quad (1.1)$$

As a result, this period is 2.23514 years and it's bigger compared to the one between Jupiter and Mars or Mars and Venus. That's why the direct transfer from Jupiter to Venus will repeat itself after every Jupiter-Mars synodic period.

Secondly, a simple way to frame the issue is to study the direct transfer between Jupiter and Venus, without performing any fly-by around Mars. It can be also useful to visualize direct transfers from Jupiter to Mars and from Mars to Venus. In Figure 1.1, Figure 1.2 and Figure 1.3 are presented three contour plots describing the costs of those direct transfers, departing during a 6 years-long window (2030-2036), barring options with a required Δv bigger than 30 km/s and calculated solving the Lambert's problem. Note that, for the Jupiter-Mars arch and for the Mars-Venus one, only Jupiter departure required Δv and Venus arrival Δv have been plotted.

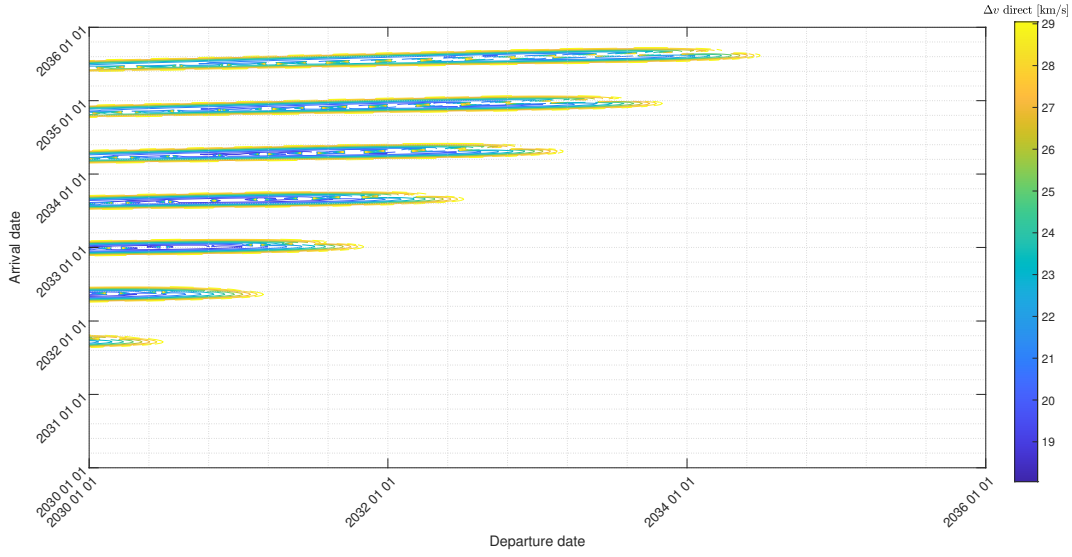


Figure 1.1: Direct Transfer for 2030-2036 departures Jupiter-Venus.

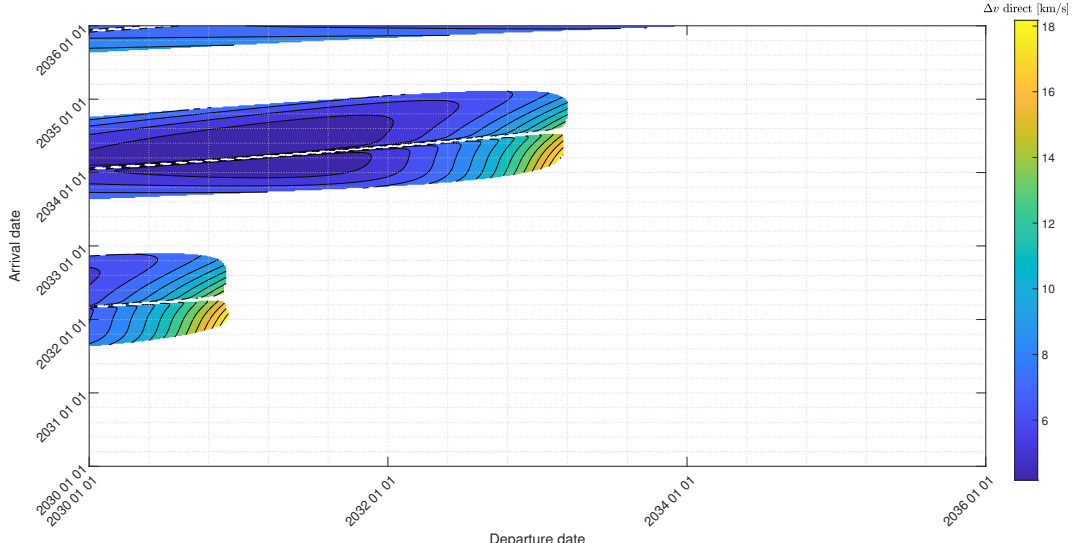


Figure 1.2: Jupiter-Mars departure Δv required.

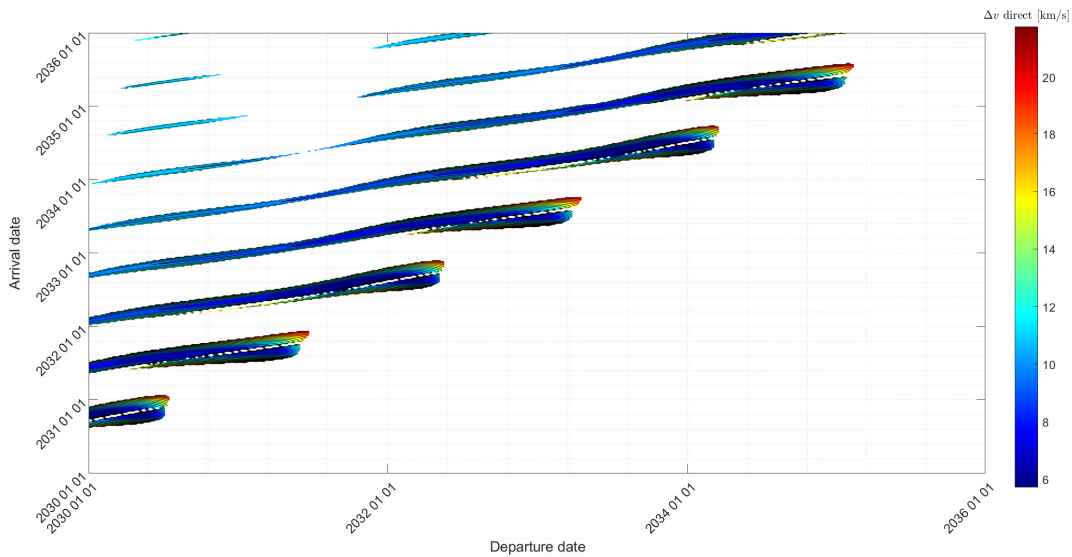


Figure 1.3: Mars-Venus arrival Δv required.

The minimum cost required for a direct transfer is around 18 km/s. This value is approximately repeated along the synodic period previously analyzed. For Jupiter-Mars transfer, the minimum Δv at departure is 4.0348 km/s, while, for Mars-Venus transfer, the minimum Δv at arrival is 5.7232 km/s.

Finally, as particular cases of direct transfers, Hohmann and parabolic transfer legs can be studied. Considering circular and co-planar orbits (which is not real because the planets have a certain inclination and eccentricity), Hohmann transfers have been calculated and characterized in order to roughly understand their times of flight and costs, which will be useful as a reference. In the same way, and compared to Hohmann transfers, parabolic trajectories are less efficient paths, but also the quicker, so minimum times of flight can be calculated from them.

In Table 1.2 may be seen, separately, both costs and times for three Hohmann transfers, as well as the minimum times related to three parabolic arcs. Parabolic trajectories have been calculated using the same departure/arrival date of the best direct transfer.

HOHMANN TRANSFER	$\Delta v_{\text{departure}} [\text{km/s}]$	$\Delta v_{\text{arrival}} [\text{km/s}]$	$\text{TOF} [\text{days}]$
Jupiter-Venus	6.606	11.385	931.64
Jupiter-Mars	4.269	5.882	1126.58
Mars-Venus	4.768	5.763	217.5
PARABOLIC TRANSFER			$\text{TOF} [\text{days}]$
Jupiter-Mars	-	-	432
Mars-Venus	-	-	75

Table 1.2: Hohmann and parabolic transfers

1.3 Grid Search

After this preliminary analysis and basing on the obtained results, it is possible to generate a grid searcher in order to found all the possible transfers, adding a powered fly-by condition

around Mars. This grid searcher takes three time windows (departure, fly-by, arrival) as vectors and it computes, in a triple "For" cycle and for each combination of dates, the total cost of the mission in terms of both Δv required and time of flight and the characteristics of the flyby. The total mission consists in solving two non-independent Lambert's problems and a powered fly-by condition around Mars. "Non-independent" means that the two Lambert's arcs are patched with the fly-by date and with the gravity assist manoeuvre, such that the final velocity of the first arc will be the heliocentric velocity before the fly-by and the initial velocity of the second arc will be equal to the spacecraft's velocity after the fly-by.

In order to reduce the computation time for the grid search and to be able to compare solutions with similar properties and reasonable times of flight, some limitations have been introduced.

Since both very short and very long transfers resulted inefficient, they have been preemptively excluded by imposing a single-arc time limitations: a minimum transfer time close to the parabolic one found before ($ToF_{min} = 432$ days for the first transfer and $ToF_{min} = 75$ days for the second arch) and a maximum transfer time similar to the Hohmann one ($ToF_{max1} = 1126$ days and $ToF_{max2} = 217$ days). A second limit is related to minimum and maximum Δv requirements. In particular, for the first transfer, solutions with a departure cost less than the Hohmann one ($\Delta v = 4.269 km/s$) and, for the second branch, options with an arrival Δv smaller than Hohmann transfer ($\Delta v = 4.768 km/s$), have been excluded. Regarding the maximum limit it is a reasonable value of ($\Delta v = 12 km/s$) for every impulse.

Moreover, as the first Lambert's arc can be calculated regardless of the arrival date, it can be performed before the third "For" cycle, significantly reducing the computation time. With all these limitations, the total CPU time is $t_{CPU} = 285.768$ s.

The whole time span has been divided into four 10 years-long departure windows. Each one has been analyzed with a grid made of 500x500x500 points in order to understand the real behaviour of the problem, to find the optimal departure, fly-by and arrival time spans and to see, eventually, a repetition of the same solution along the years.

Here the results of this analysis are presented in four porkchop plots, where the fly-by transfers are shown and compared with the direct transfers. The porkchop plots relating to the fly-by transfer options have been made projecting the 3D matrix of the grid analysis onto a plane: every point has a fixed departure and arrival date and it represents the minimum Δv for the fly-by possible dates within the combination departure - arrival.

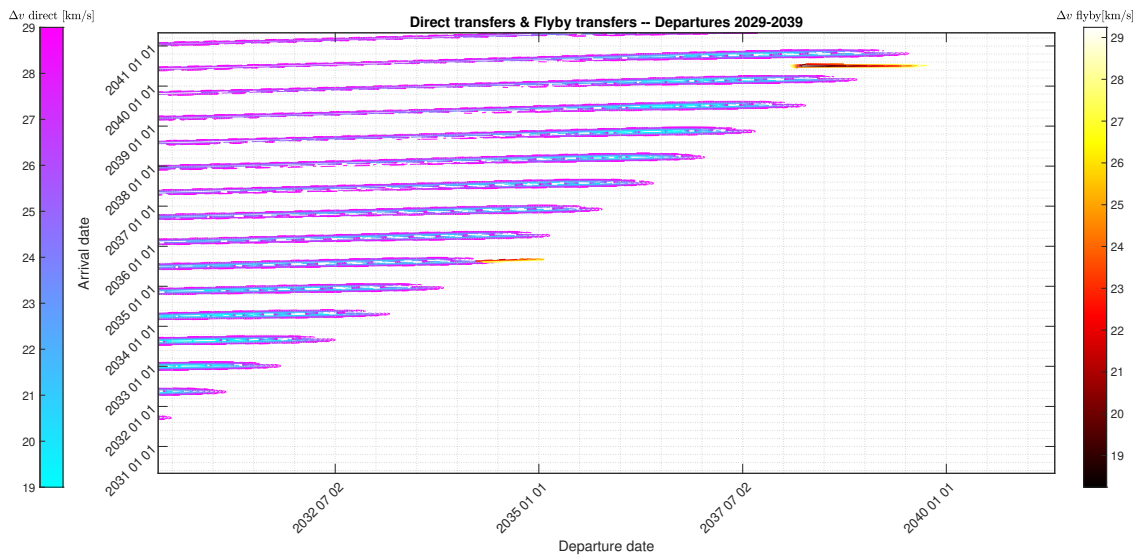


Figure 1.4: 2029-2039 departures

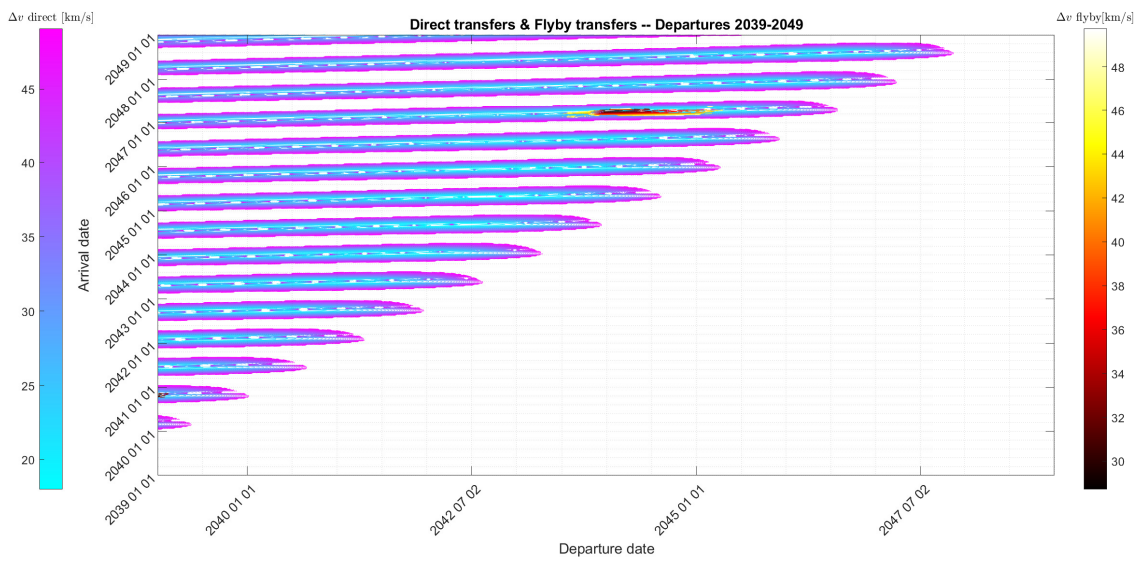


Figure 1.5: 2039-2049 departures

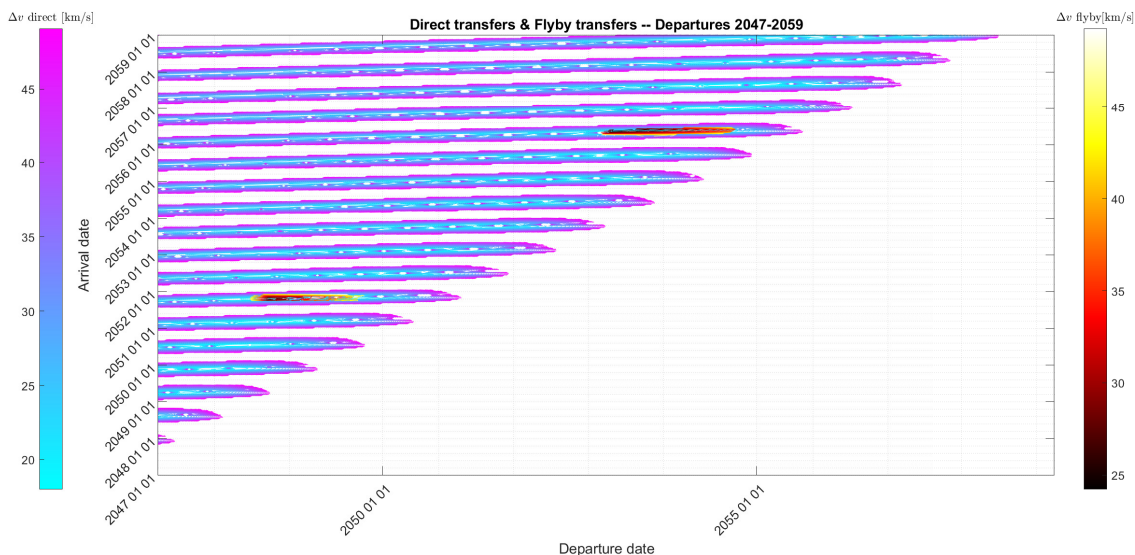


Figure 1.6: 2047-2059 departures

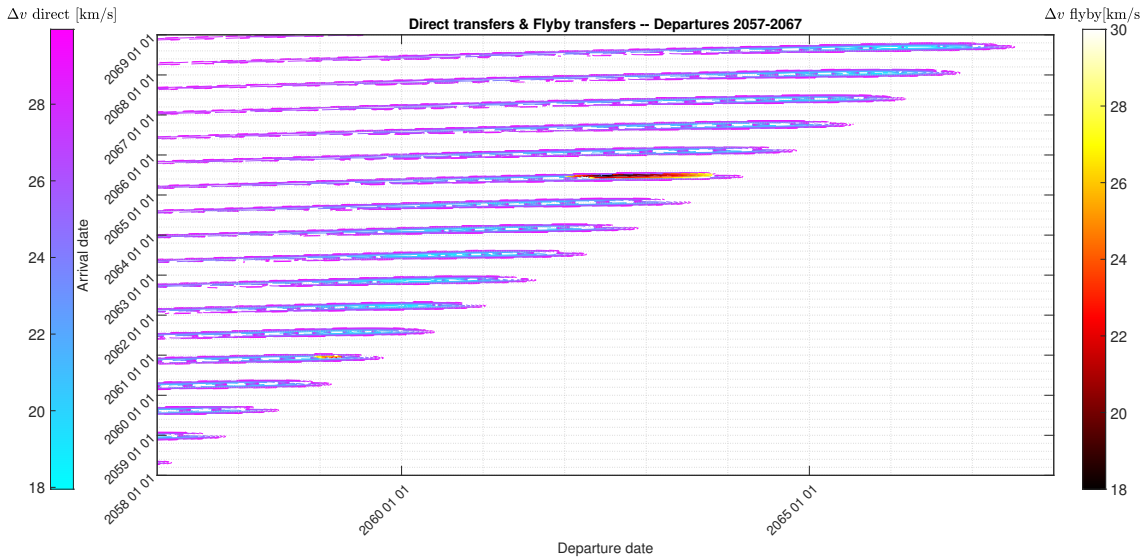


Figure 1.7: 2057-2069 departures

In Table 1.3 are presented the best results of the grid analysis for each of the four intervals

Departure window	Δv_{\min} [km/s]	Departure date	Fly-by date	Arrival date
2037/04-2038/12	18.2421	2037/09/22	2040/07/12	2040/10/23
2048/01-2049/05	24.7768	2048/07/4	2051/07/04	2051/10/27
2059/01-2059/08	20.6513	2059/03/3	2060/08/30	2060/12/11
2062/03-2063/02	16.6043	2062/05/16	2065/03/15	2065/06/27

Table 1.3: Transfer options with Fly-By

1.4 Optimization

The initial grid search has been used as the foundation for the optimization process. The most promising regions were further analyzed by means of an even finer grid and a selection of optimization algorithms.

The grid refinement has been accomplished restricting the time interval in the proximity of a good solution maintaining the same number of points (500x500x500), thus obtaining a higher density. By taking the two best results in terms of Δv from Table 1.3 and imposing a 1 year time window around them the following results are obtained (Table 1.4). Both show a small yet appreciable reduction of the cost of the manoeuvre.

Δv [km/s]	Departure date	Fly-by date	Arrival date
17.855	05-Jul-2037	09-Jul-2040	19-Oct-2040
16.291	06-May-2062	15-Mar-2065	24-Jun-2065

Table 1.4: Optimized Grid-Search results

In order to verify and possibly improve these results it has been decided to feed them as an initial guess into a gradient-based optimization tool. The problem has been written

as a *GlobalSearch* problem and optimized through the *fmincon* solver. The lower and upper boundaries have been maintained the same as the ones used for the finer grid search. The outputs of the optimization program are reported in Table 1.5. Again, a small improvement over previous results is visible.

Δv [km/s]	Departure date	Fly-by date	Arrival date
17.473	21-Jan-2037	04-Jul-2040	19-Oct-2040
16.283	06-May-2062	15-Mar-2065	23-Jun-2065

Table 1.5: GlobalSearch optimization results

The data reported in Table 1.6 is the result of the analysis of the same regions with a genetic algorithm. Since this algorithm may return a different solution each time, the same analysis has been repeated several times to be sure to get consistent results. For this reason the problem has been written in vectorized form to reduce computation time.

Δv [km/s]	Departure date	Fly-by date	Arrival date
17.850	09-Jul-2037	08-Jul-2040	18-Oct-2040
16.450	01-Jul-2062	17-Mar-2065	23-Jun-2065

Table 1.6: Genetic algorithm optimization results

1.5 Conclusion and solution selection

The figure of merit for choosing the best solution is the total cost of the transfer in terms of Δv . Based on that criterion, the ideal solution between the ones analyzed comes from the *GlobalSearch* algorithm and is summarized in Table 1.7.

Departure date	06-May-2062, 14:34:16
Fly-by date	15-Mar-2065, 17:29:56
Arrival date	23-Jun-2065, 13:27:34
Total Δv [km/s]	16.2833
Δv required at departure [km/s]	5.9303
Δv required for powered fly-by [km/s]	0.000049
Δv required at arrival [km/s]	10.3530
Impact parameter (aiming radius) [km]	3735.6435
Fly-by altitude [km]	162.0937
Time spent inside Mars' SOI [hours]	21.79
Mars' SOI radius at fly-by [km]	592176.0555
Time of flight (ToF)	3 years, 1 month, 17 days

Table 1.7: Transfer with lowest Δv

The first thing to notice is that this solution is cheaper than the direct transfers from Jupiter to Venus that have been computed, thus making the fly-by a viable option. The total transfer

time of roughly 3 years makes this transfer slower than a direct one but it is still very reasonable. While the mission is completed within the assigned time boundaries using this solution, it must be noticed that the departure is quite late: if an earlier departure is preferred, then the transfer starting in 2037 (see Table 1.5) might be considered as an alternative option with only slighter bigger Δv .

From Figure 1.8 it is evident that the shape of the mission's trajectory closely resembles that of an Hohmann-like transfer from Jupiter to Venus, with Mars being somewhere in the middle making the fly-by possible. This justifies the very low cost of the powered gravity assist manoeuvre.

According to the graphics in [Braeunig \(2017\)](#), Mars' atmosphere should be extremely rarefied at the computed fly-by altitude of 162 km, so the manoeuvre shouldn't be impeded by air drag. If the study of the mission were to be carried on in greater detail, it might be appropriate to set a higher limit for the minimum altitude to provide a better safety margin. For instance, the solution obtained through the genetic algorithm (1.6) ensures a higher altitude (406 km) for a small increment in Δv .

Figure 1.9 and Figure 1.10 show the incoming and out-coming hyperbolic arcs inside Mars' SOI (note that only a fraction of the SOI is pictured for better visibility).

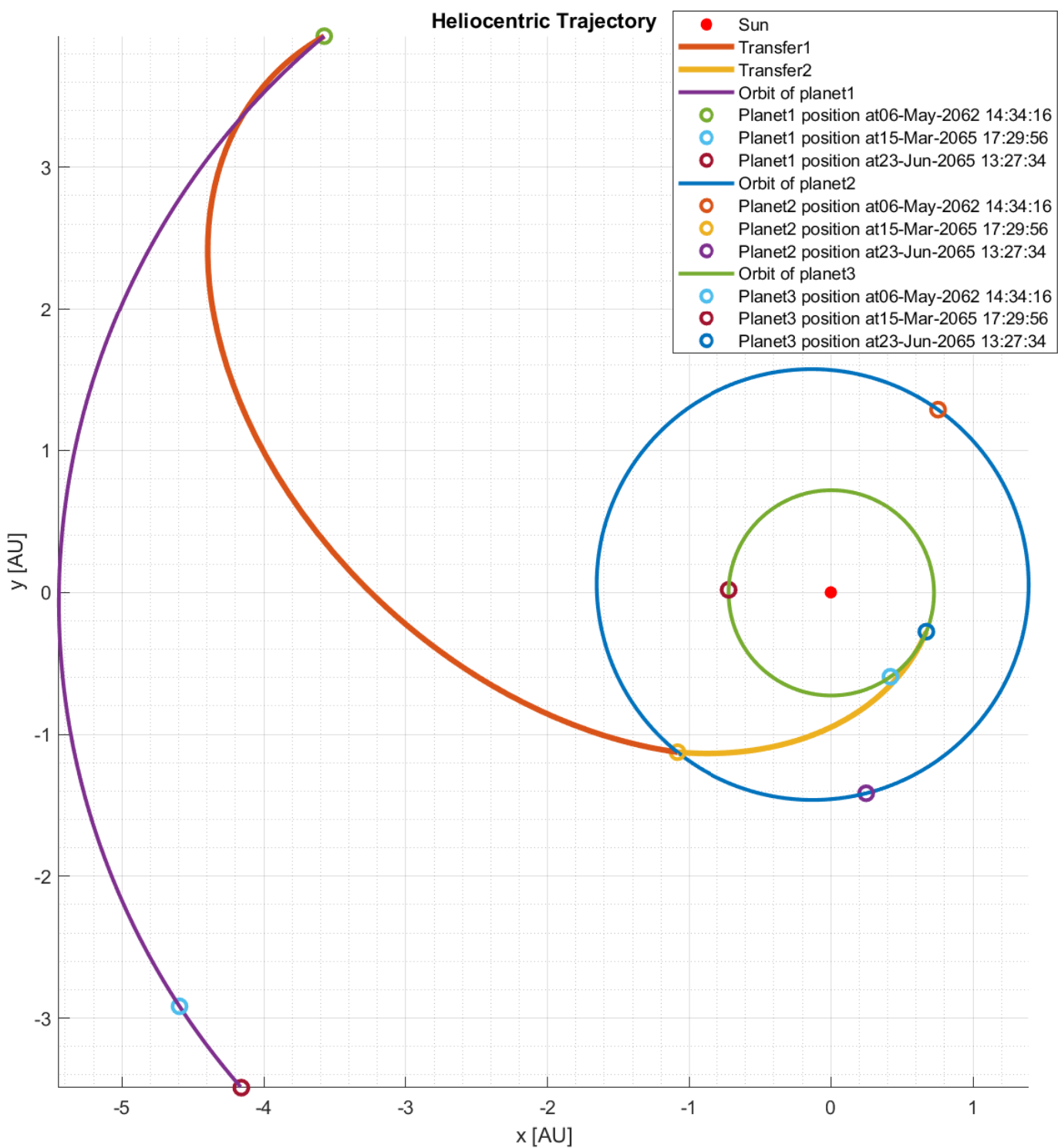


Figure 1.8: Transfer trajectory in heliocentric frame

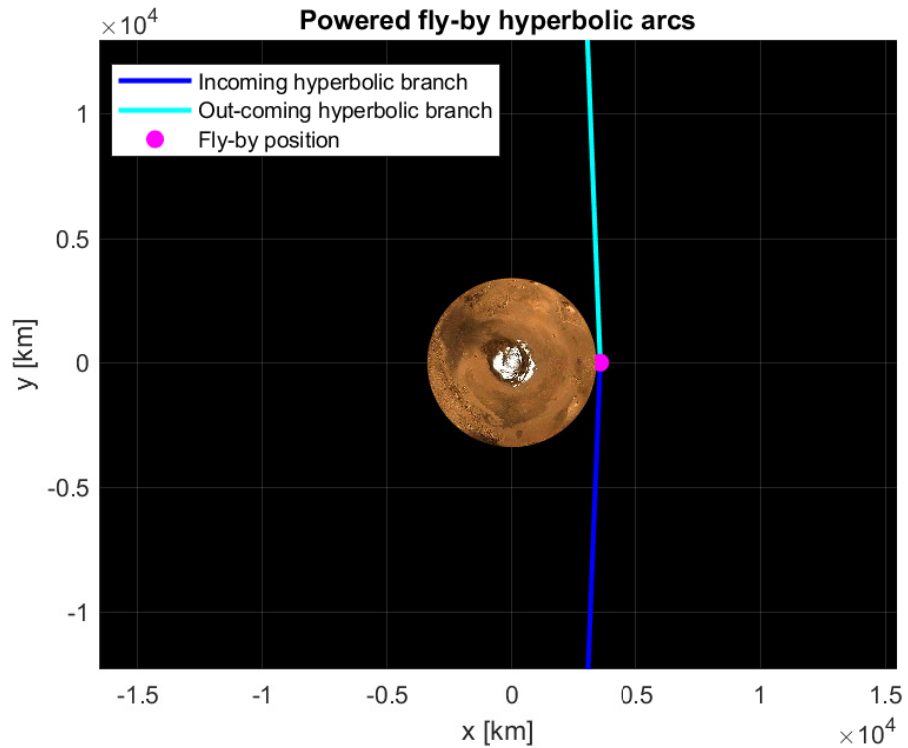


Figure 1.9: Fly-by trajectory in perifocal frame

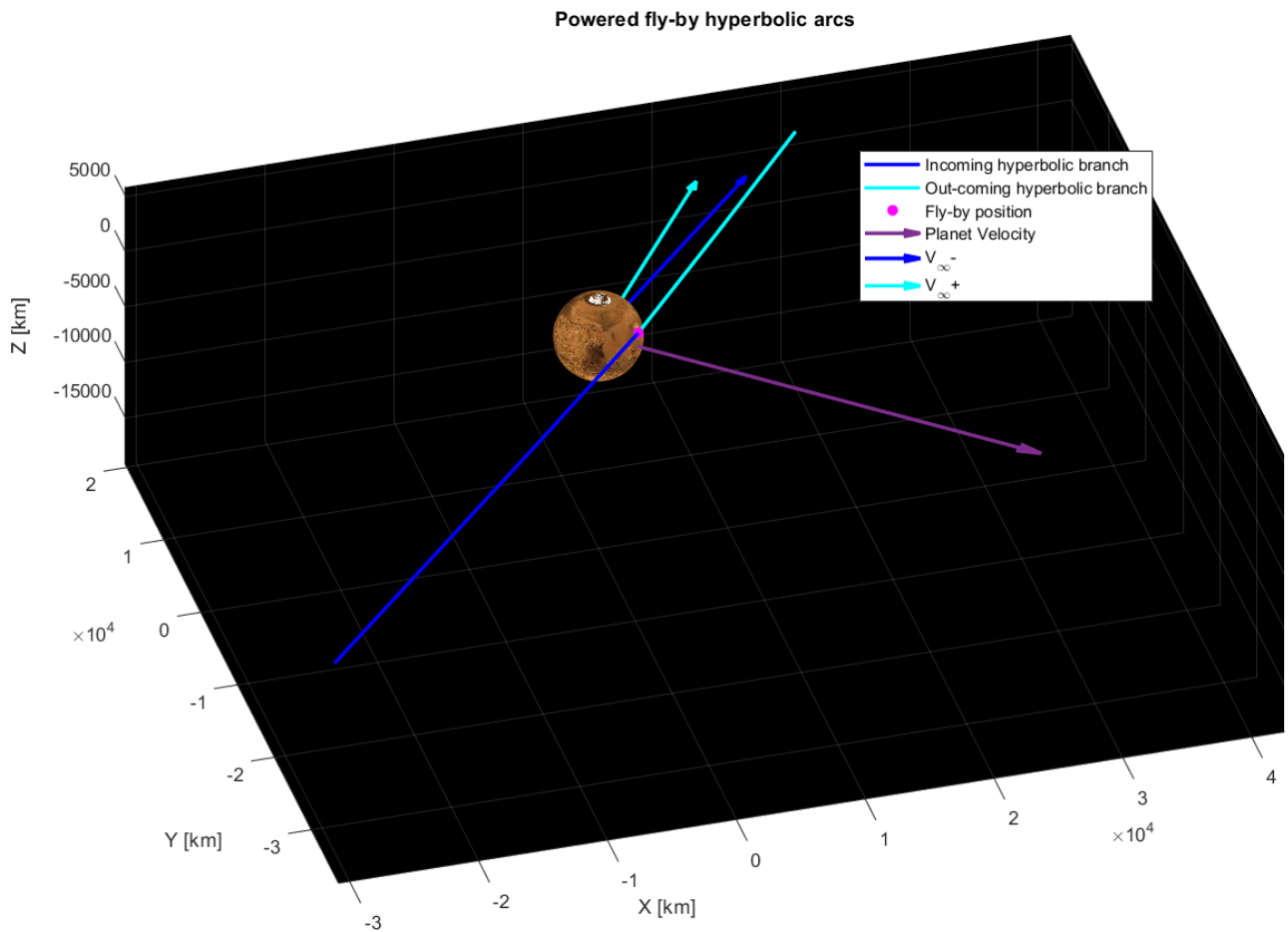


Figure 1.10: Fly-by trajectory highlighting Mars' velocity and s/c velocities at infinite

CHAPTER 2

Planetary Orbit

2.1 Introduction

To carry out an analysis on ground track plots and orbit perturbations of Earth-centered orbits, the parameters in Table 2.1 are the ones that have been assigned or chosen. Aside of the given perturbation to study, the J2 effect of Earth's oblateness will be considered.

Parameter	Value
$a[\text{km}]$ (assigned)	$3.3923 \cdot 10^4$
e (assigned)	0.2991
$i[\text{deg}]$ (assigned)	23.2497
Perturbation (assigned)	Moon
$\Omega[\text{deg}]$	0
$\omega[\text{deg}]$	0
$\theta_0[\text{deg}]$	0

Table 2.1: Parameters assigned and chosen for mission.

2.2 Ground Track

As requested, the ground track has been calculated for 1 orbit, 1 day and 10 days. In each of them, the comparison between ground track computed with or without J2 effect are shown.

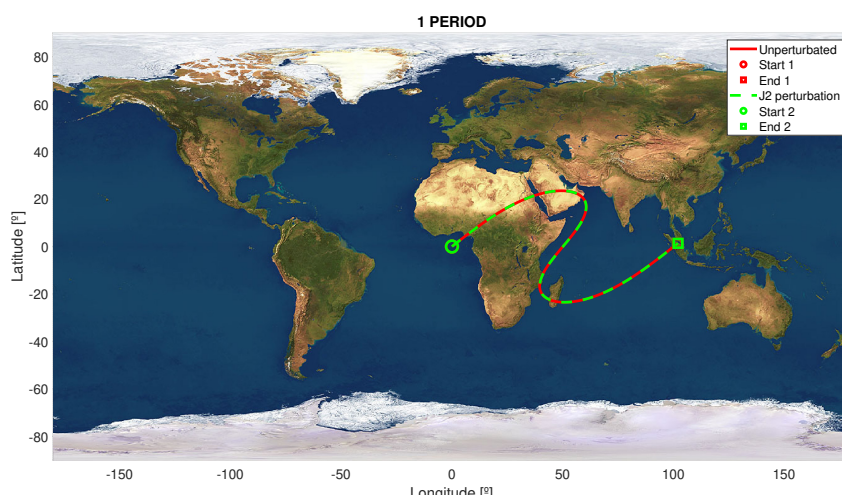


Figure 2.1: 1 Orbit ground track with and without J2 effect

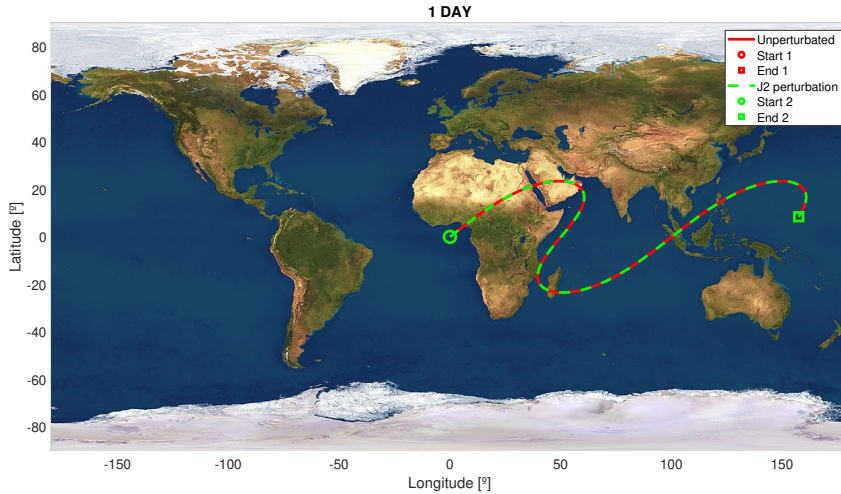


Figure 2.2: 1 Day ground track with and without J2 effect

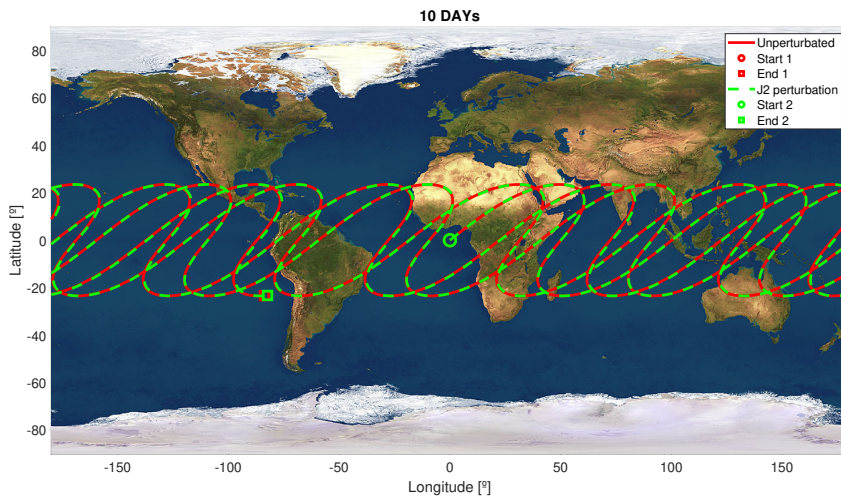


Figure 2.3: 10 Days ground track with and without J2 effect

Nevertheless, this short period of time is not enough to appreciate the change produced by the J2 perturbation. The main issue appreciated is an advancement of the RAAN of the orbit with J2 effect respect to the orbit without it, but mostly impossible to distinguish in 10 days. More days would make the drawing too confusing to appreciate any details.

As a second step, a repeating ground track based on the original semimajor axis is calculated and plotted. This has been made, again, by ideal orbit propagation and J2 conservation.

- 1. Repeating Ground Track with no perturbations:** for given k (revolutions of the planet) and m (revolutions of the satellite), assuming no perturbations, the new a of the orbit is calculated as in (2.1).

$$n = \frac{2\pi}{T} = \sqrt{\frac{\mu}{a_{RGT}^3}} = \omega_E \frac{k}{m}; \quad (2.1)$$

From (2.1), the value of a_{RGT} is obtained directly. For the case of $k = 7$ and $m = 5$, the result is $a_{RGT} = 33692\text{km}$.

2. **Repeating Ground Track with J2 effect:** now as the oblateness of the Earth has to be accounted for, the new equation results in (2.2). The values of the secular evolution of the parameters is defined using the Gauss planetary equations and expressed in terms of a in (2.3)

$$n = \sqrt{\frac{\mu}{a_{RGT}^3}} = \frac{k(\omega_E - \dot{\omega})}{m} - \dot{\omega} - \dot{M}_0 \quad (2.2)$$

$$\begin{cases} \dot{\Omega} = -\left[\frac{3}{2}\frac{\sqrt{\mu}J_2R_e^2}{(1-e^2)^2a^{7/2}}\right]\cos i \\ \dot{\omega} = -\left[\frac{3}{2}\frac{\sqrt{\mu}J_2R_e^2}{(1-e^2)^2a^{7/2}}\right]\left(\frac{5}{2}\sin^2 i - 2\right) \\ \dot{M}_0 = -\left[\frac{3}{2}\frac{\sqrt{\mu}J_2R_e^2}{(1-e^2)^2a^{7/2}}\right]\left(1 - \frac{3}{2}\sin^2 i\right) \end{cases} \quad (2.3)$$

Solving using as initial value on the iteration a_{RGT} from the previous calculation, the result is $a_{RGTJ2} = 33691\text{km}$, which is very similar to the initial value.

The ground track obtained as a result for both calculations are showed in Figure 2.4 for 10 days.

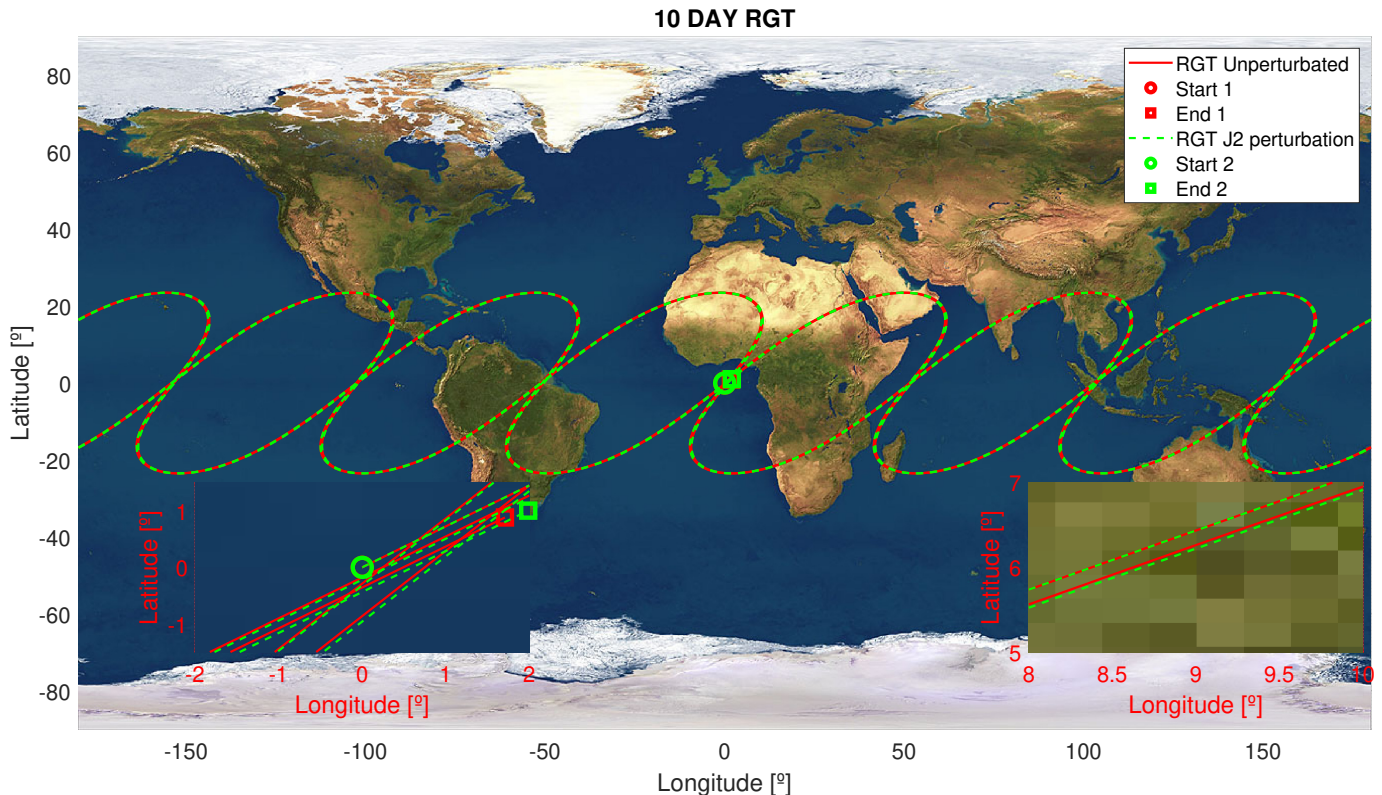


Figure 2.4: 10 Days ground track with and with J2 effect

2.3 Moon Perturbation

Back to the original orbit of the assigned satellite, in that region the strongest perturbation is the third body perturbation due to the Moon. The total acceleration over the satellite is

expressed in (2.4) in the inertial reference system. This acceleration is due both to the main body (Earth) and the third body (Moon). In this notation, r is the vector between the main body and the spacecraft and r_M the vector from the main body to the Moon (which is the information known from the ephemeris). The distance between the satellite and the Moon will be $|r_M - r|$.

$$\mathbf{a} = \frac{\mu_E}{r^3} \mathbf{r} + \frac{\mu_M}{|r_M - r|^3} (\mathbf{r}_M - \mathbf{r}) - \frac{\mu_M}{r_M^3} \mathbf{r}_M \quad (2.4)$$

Therefore, the perturbation terms are the two last ones, which did not appear in the unperturbed equation. The first one is the direct effect of the third body on the spacecraft, whereas the second one is the effect of the third body on the main body, which indirectly affects the spacecraft's motion. For Earth satellites, it verifies $r \ll r_M$; the second order terms in r/r_M may be eliminated from the equation, giving the final equation of the perturbations as (2.5), which is expressed in the inertial frame of reference.¹

$$\mathbf{a}_M = \frac{\mu_M}{r_M^3} \left(-\mathbf{r} + 3 \frac{\mathbf{r}_M \cdot \mathbf{r}}{r_M^2} \mathbf{r}_M \right) \quad (2.5)$$

If the integration of the equation of motion is done through the Kepler equation, this term is directly added as an acceleration on the spacecraft. To calculate the appropriate r_M , the date for calculating the ephemeris is given for each time step, resulting the final equation as in (2.6). The integration of this equation is done in MATLAB in $t_{CPU} = 0.3972$ seconds in approximately 11000 time steps computed with a precision of 10^{-10} for a time span of 60 days.

$$\ddot{\mathbf{r}} = \frac{\mu}{r^3} \mathbf{r} + \mathbf{a}_{J2} + \mathbf{a}_M \quad (2.6)$$

On the other hand, integrating using the Gauss planetary equations requires an extra step of transferring the acceleration from inertial reference of frame to (t, n, b) , so that way the input for Gauss planetary equations ([Vallado \(2001\)](#), equation (8-24)) is $\mathbf{a}_P = \mathbf{a}_{J2} + \mathbf{a}_M = (a_t, a_n, a_b)$.

The integration of this equation is done in MATLAB in $t_{CPU} = 0.9240$ seconds in approximately 6400 time steps computed with a precision of 10^{-10} for a time span of 60 days. The meaning of this numbers compared to the Kepler integration gives an interesting result: Gauss equations require less dense time intervals to achieve the same precision. This indicates that Gauss equations are more suitable for a precise integration. Nevertheless it takes more time due to two factors:

- The rotation of the perturbation acceleration is an extra calculation that is performed at each time step, therefore increasing computation time. Other perturbations such as drag are already expressed in the adequate coordinate system, thus being easier to integrate.
- There are six scalar equations instead of one vectorial, which is faster to compute for MATLAB.

¹See more detailed development in [Sanz-Aránguez \(1999\)](#)

The result for the integration of Kepler equations is showed in Figure 2.5. Essentially, for 60 days the integration with Gauss equations is very similar, so Figure 2.6 shows the difference for the orbital parameters in each time step. The greatest difference when comparing both results comes in a , where it reaches a maximum of about 10^{-2} . None of the parameters' difference between integrations has, apparently, a drift in time. Therefore, it is concluded that they are equivalent in the long term.

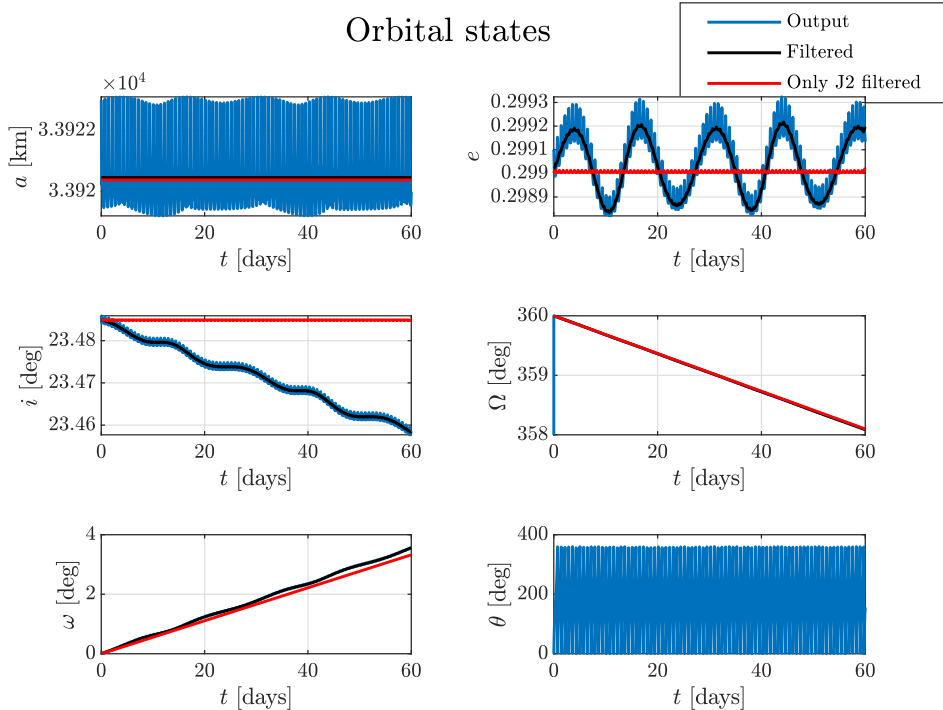


Figure 2.5: Orbital parameters as integrated with Kepler equations in 60 days.

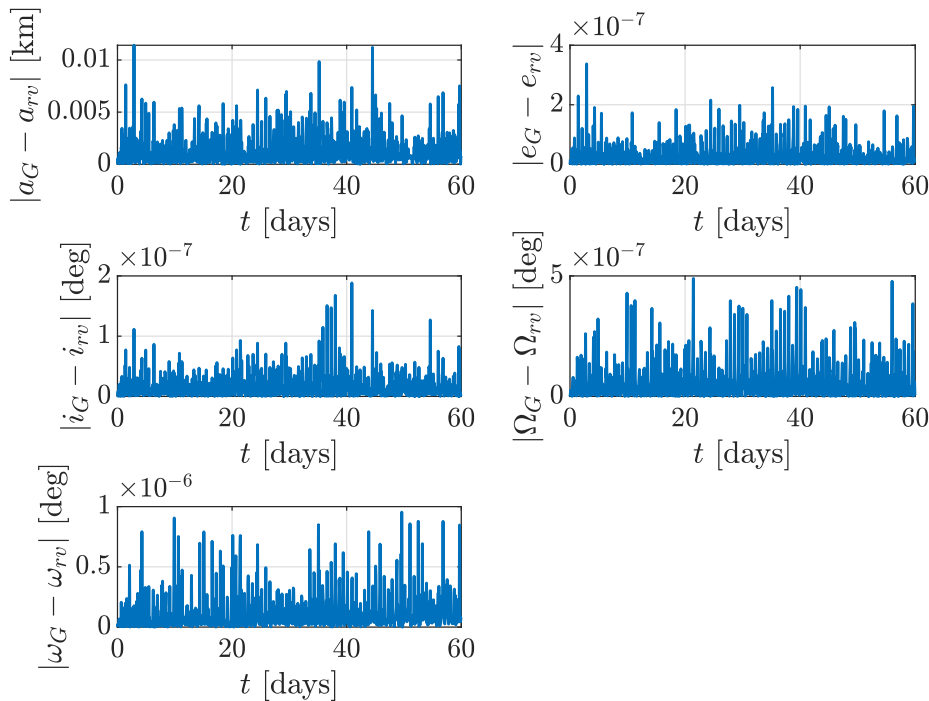


Figure 2.6: Orbital parameters comparison between Gauss and Kepler integration. Filter used: moving average based on period time

2.4 Element evolution and Filtering

Orbital elements are affected by J2 and Moon perturbation at every time scale, indeed it is possible to look at oscillations whose period is in order of days, months or years. For example Moon perturbations have a period of approximately 28 days, which is coincident with the revolution time of the Moon around the Earth. Looking at Figure 2.6 this fact is not so clear since eccentricity seems to have the half of this period. Despite the 2 oscillations seem to have the same amplitude, looking carefully it is possible to notice that they are not the same. Therefore it is confirmed that 28 days is the repetition period for low-frequency eccentricity, inclination and argument of perigee oscillations. Moon main secular effects are on i , e , ω , Ω . However Earth oblateness acts on these two last parameters too, leaving a , e , i unchanged, and its secular effects are so much stronger on ω and Ω . As expected, J2 perturbation is always the strongest effect on Earth centered orbits.

All of the secular effects have been studied for a time span which has been considered comparable to a real disposal time of 10 years. Results are shown in Figure 2.7.

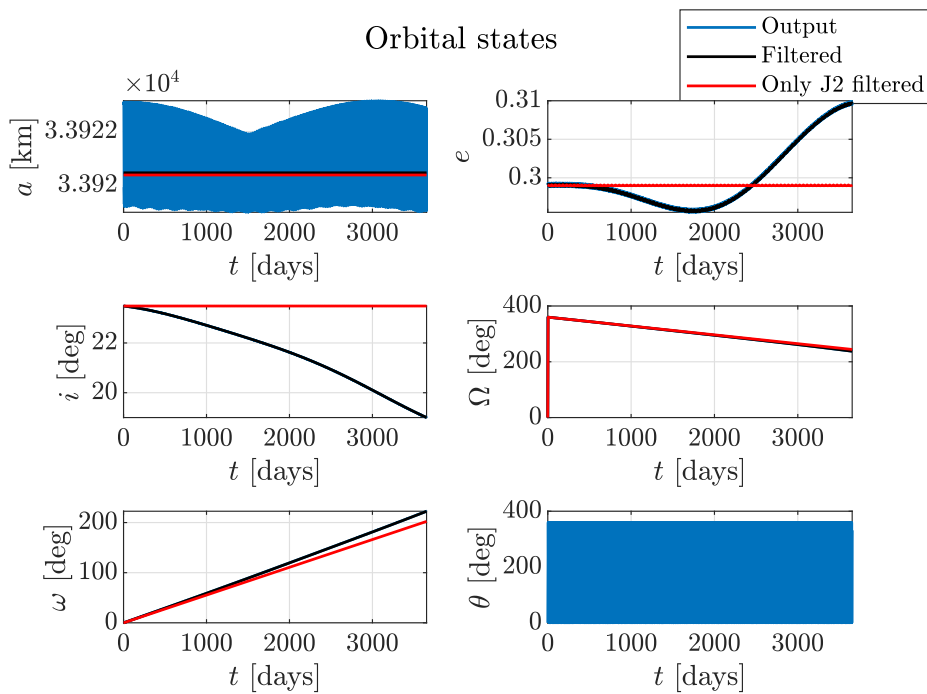


Figure 2.7: Evolution of the orbital elements for 10 years (starting from 29/12/2000). Filter used: moving average based on time period.

Going back at Eqs. 2.3 it is possible to do some consideration for the orbit that has been chosen:

- Since the orbit is prograde ($i = 23.2497^\circ$), $\dot{\Omega} < 0$ therefore J2 effect moves RAAN westwards (nodal precession).

- Since $i < 63.4^\circ$, $\dot{\omega} > 0$ therefore J2 effect causes a perigee precession effect, advancing it to higher values. This is the same effect that, on the repeated ground track, tends to advance the perigee and therefore the final point ends up at a higher latitude after an integer number of repetitions.

When thinking about disposal, it has to be kept in mind that, if the orbit does not decay with time, due to current regulations a de-orbiting maneuver will be performed. This might be done either to a graveyard orbit or to Earth-collision course.

Among other effects, the most important secular variations provoked by the moon involve the inclination and the eccentricity. Nevertheless, the variation on eccentricity is small and in a span of 10 years. Inclination also does not vary much, but its variation is appreciated even in short term (60 days).

2.5 Comparison with real data

The satellite chosen to compare the propagator with the real data is the Chinasat7. In Table 2.2 are displayed the parameters of the assigned spacecraft and Chinasat7. Because its orbital parameters are similar, it is also located within a region where the Moon perturbation has a greater impact than other effects on the orbital parameters drift. The analysis or the evolution of the orbital elements of this satellite has been carried using MATLAB and GMAT² to compare with real data.

Orbital parameters	Assigned	Chinasat 7
a[km]	$3.3923 \cdot 10^4$	$4.04647 \cdot 10^4$
e	0.2991	0.3098
i[deg]	23.2497	27.9436

Table 2.2: Parameters assigned compared to Chinasat7 from [SAIC \(2020\)](#).

All the orbital elements have been computed again for these new initial condition of Chinasat7 from 01/01/2010 to 28/12/2020 as shown in Figure 2.8.

²NASA (2016) and NASA (2012)

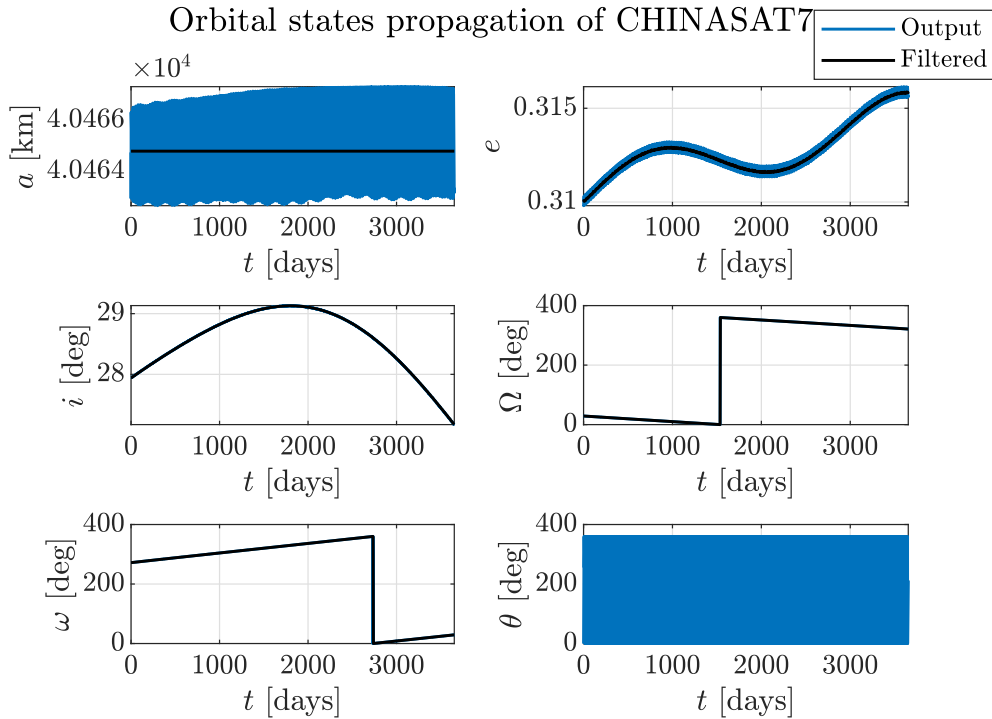


Figure 2.8: Propagation of orbital elements with Chinasat7 data taken starting from 29/12/2000 by [SAIC \(2020\)](#). Filter used: moving average based on number of points.

Data regarding orbital elements have been downloaded for the same time span in order to compare the results achieved with MATLAB respect with those of the real satellite. These plot are shown in Figure 2.9.

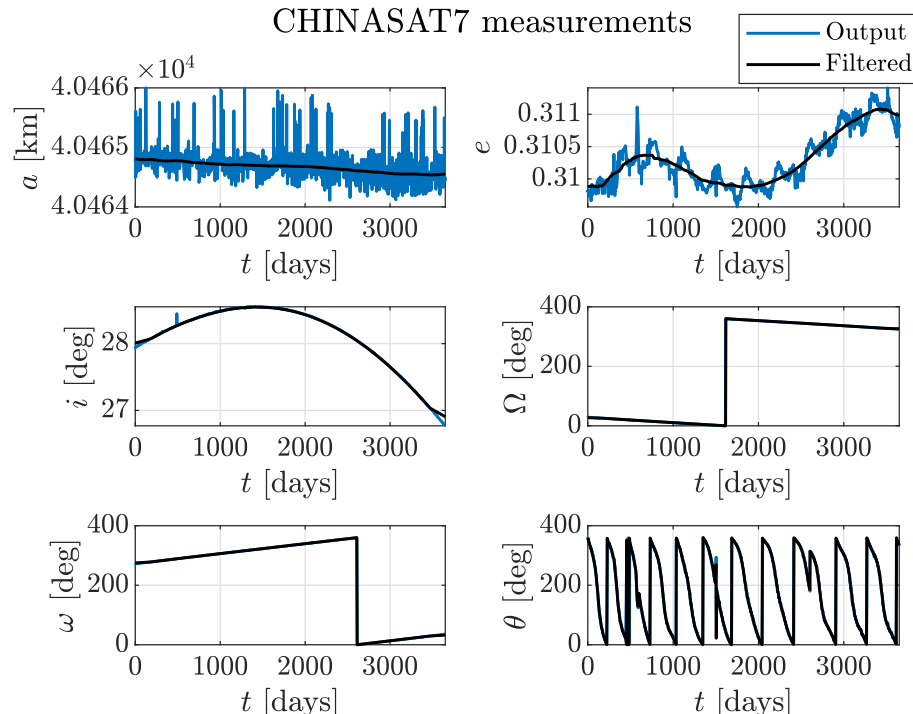


Figure 2.9: Chinasat7 satellite orbital elements with time. Filter used: moving average based on number of points.

As it can be seen there are a lot of similarities both in a qualitative way and in a quantitative way in every plot. However there are also few differences, for example the slight decreasing of the semi-major axis (even if almost negligible), the eccentricity bigger value and a slightly bigger value on the inclination peak. Despite none of those differences is so evident to highlight some remarkable error in the program, GMAT has been used with both perturbations of J2 and Moon to have an additional comparison with MATLAB results.

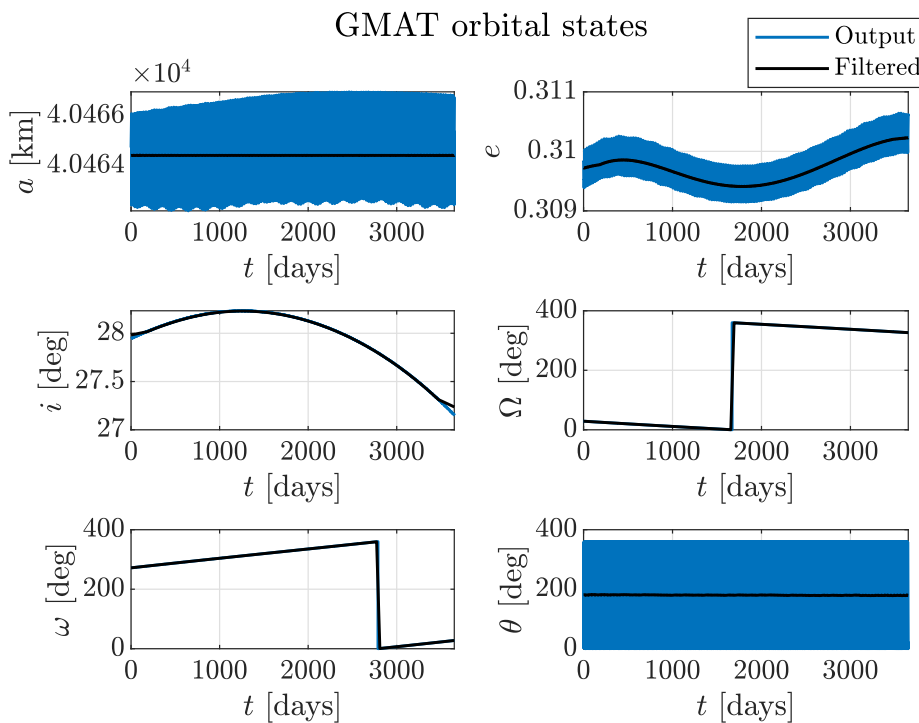


Figure 2.10: Propagation of orbital elements with GMAT. Filter used moving average moving average based on n° points

Results of GMAT agree with the ones from MATLAB except for the eccentricity plot which seems to be more similar to the real satellite's one. This kind of error is probably due to different integrator used for propagation or a different model for ephemeris (which acts on the position of the Moon).

A Runge-Kutta 89 has been implemented to solve this source of error and it proved that the error is mainly to the integrator, whose error has been increased with time. Therefore the program after almost 800 days started to give wrong results on eccentricity. Of course, results are still far from being perfect, as small changes in ephemeris, mass o rotation speed give diverging results with time. Also, it is relevant to keep in mind that the satellite is effected by all the perturbations, including solar radiation pressure, which might also be relevant within the region it is located.

For a better understanding of the accuracy of the results, mean value, standard deviation and maximum error percentage between the real satellite's data and both the MATLAB and GMAT propagations have been computed. The results are in Table 2.3.

Orbital element	Mean value	STD	Max error
a	$4.04645 \cdot 10^4$	0.0064	0.2521
	$4.04644 \cdot 10^4$	0.0134	0.2005
e	0.312752	0.0014	0.0049
	0.309729	$2.4046e-4$	$9.0313e-4$
i	28.5685	0.5097	0.7062
	27.9672	0.02856	0.3309
Ω	259.61	0.5917	0.1010
	252.44	0.5764	0.0133
ω	274.36	0.3395	0.0863
	277.09	0.3089	0.0329

Table 2.3: Colored row: filtered program results vs. filtered satellite data
 White line: filtered GMAT results vs. filtered satellite data

Bibliography

- Braeunig, R. A. (2017). *The Martian Atmosphere*. <http://www.braeunig.us/space/atmmars.htm>. [Accessed: 01.01.2021]. 9
- NASA (2012). *GMAT user guide*. <http://gmat.sourceforge.net/docs/R2012a/help-letter.pdf>. [Accessed: 20.01.2021]. 18
- NASA (2016). *General Mission Analysis Tool (GMAT)*. <https://software.nasa.gov/software/GSC-17177-1>. 18
- SAIC (2020). *Space-track*. <https://www.space-track.org/>. [Accessed: 01.01.2021]. 18, 19
- Sanz-Aránguez, P. (1999). *Notes of the course Space Vehicles*. ETSIAE-UPM. 15
- Vallado, D. A. (2001). *Fundamentals of astrodynamics and applications*, volume 12. Springer Science & Business Media. 15